

**PCCP****Manipulating Triplet States: Tuning Energies, Absorption, Lifetimes, and Annihilation Rates in Anthanthrene Derivatives**

Journal:	<i>Physical Chemistry Chemical Physics</i>
Manuscript ID	CP-ART-09-2018-006048.R1
Article Type:	Paper
Date Submitted by the Author:	29-Oct-2018
Complete List of Authors:	Stewart, David; Air Force Research Laboratory Materials and Manufacturing Directorate, Shi, Jianmin; US Army Research Laboratory Naranjo, Tristan; Air Force Research Laboratory Materials and Manufacturing Directorate Grusenmeyer, Tod; Air Force Research Laboratory Materials and Manufacturing Directorate Artz, Jacob; Air Force Research Laboratory Materials and Manufacturing Directorate, McCleese, Christopher; Air Force Research Laboratory Materials and Manufacturing Directorate O'Donnell, Ryan; US Army Research Laboratory Cooper, Thomas; Air Force Research Laboratory Materials and Manufacturing Directorate, Shensky, William; US Army Research Laboratory, Haley, Joy; Air Force Research, Laboratory, Materials and Manufacturing Directorate

SCHOLARONE™  
Manuscripts

# Manipulating Triplet States: Tuning Energies, Absorption, Lifetimes, and Annihilation Rates in Anthanthrene Derivatives

*David J. Stewart,<sup>a,b</sup> Jianmin Shi,<sup>c</sup> Tristan R. Naranjo,<sup>a,d</sup> Tod A. Grusenmeyer,<sup>a</sup> Jacob M. Artz,<sup>a,e</sup>*

*Christopher L. McCleese,<sup>a</sup> Ryan M. O'Donnell,<sup>c</sup> Thomas M. Cooper,<sup>a</sup> William M. Shensky III,<sup>c</sup> and Joy E.*

*Haley<sup>\*a</sup>*

<sup>a</sup>Air Force Research Laboratory, Materials and Manufacturing Directorate, Functional Materials Division,  
Wright-Patterson AFB, Ohio 45433-7750, United States

<sup>b</sup>General Dynamics Information Technology, 5100 Springfield Pike, Dayton, Ohio 45431, United States

<sup>d</sup>U.S. Army Research Laboratory, 2800 Powder Mill Road, Adelphi, Maryland 20783-1138

<sup>e</sup>Department of Physics, United States Air Force Academy, U.S. Air Force Academy, Colorado 80840,  
United States

<sup>e</sup>Southwestern Ohio Council for Higher Education, Dayton, Ohio 45420, United States

ABSTRACT: The photophysical properties of anthanthrene, four anthanthrene derivatives containing varying phenyl and *p*-*t*Bu-phenyl substituents, and two anthanthrones with phenyl and *p*-*t*Bu-phenyl substituents are examined. In general, as the anthanthrenes and anthanthrones become more substituted, red-shifts are observed in the peak maxima of the ground- and excited-state absorption and fluorescence spectra. The anthanthrones have large ( $> 0.8$ ) intersystem crossing (ISC) quantum yields ( $\Phi_T$ ) likely caused by  $n\pi^*$  character in the ground or excited states. A bromo-substituted anthanthrene has a unity ISC yield due to an ISC rate constant of  $2.5 \times 10^{10} \text{ s}^{-1}$  caused by heavy-atom induced, spin-orbit coupling. This leads to low fluorescence quantum yields ( $\Phi_F$ ) in these three derivatives. The parent anthanthrene and remaining derivatives behave much differently. All have  $\Phi_F$  values from 0.58 – 0.84 with lower  $\Phi_T$  values as radiative decay outcompetes ISC. The anthanthrones have remarkable excited-state absorption with strong, broad transitions across the visible with weaker transitions extending to nearly two  $\mu\text{m}$ . The anthanthrenes have very similar-shaped, broad transitions in the visible which can be shifted  $\sim 60 \text{ nm}$  by controlling the substituents. The triplet lifetimes range from 31 – 1200  $\mu\text{s}$  and increase as the ISC yields decrease; the bromo-substituted anthanthrene is shortest, followed by the anthanthrones then the other anthanthrenes. The rate of triplet-triplet annihilation is also effected by the presence of substituents; as the amount of steric bulk is increased, the rate of annihilation decreases.

## Introduction

Excited-state absorption (ESA) plays a critical role in the effectiveness of nonlinear optical processes such as reverse-saturable absorption<sup>1-6</sup> (RSA) and effective-three-photon absorption<sup>7-11</sup> (E3PA). RSA occurs when the ESA has a larger extinction coefficient than the ground state, leading to higher optical density in the excited state at a given wavelength. E3PA occurs when a two-photon absorbing material also has significant ESA whereby a third sequential photon can be absorbed after the simultaneous two-photon excitation, which can greatly enhance the nonlinearity. Therefore, the intensity and wavelength of the ESA have direct influence on the performance of RSA and E3PA materials. Additionally, materials that have long excited-state lifetimes are preferable due to their ability to perform over larger temporal windows. Accordingly, being able to control the intensity and energy of the ESA, as well as the excited-state lifetime is a distinct advantage when designing nonlinear absorbing materials.

The triplet-triplet absorption (TTA) spectra and lifetimes of a number of organic hydrocarbons have been catalogued over the past several decades.<sup>12-14</sup> Anthracene has been widely studied but has a relatively narrow TTA band at high energy. Adding chloro, bromo, or cyano groups to anthracene can slightly red-shift the TTA.<sup>15</sup> Other substituted anthracenes such as 9,10-diphenylanthracene (445 nm) show only moderate shifts relative to the parent.<sup>16</sup> Increasing aromaticity/size typically red-shifts TTA, as the maxima of anthracene, tetracene, and pentacene in benzene are 430, 465, and 505 nm, respectively.<sup>12</sup> Additionally, steric bulk and/or substitution position can inhibit collisional deactivation via triplet-triplet annihilation and allow triplets to persist longer.<sup>17-22</sup> However, the limited knowledge of how to tune ESA renders continued investigation in this area important. Anthanthrene<sup>23</sup> has a broader and red-shifted triplet-triplet absorption spectrum relative to anthracene, and could therefore be more useful as an RSA or E3PA material. In this report, we investigate the photophysical properties of several anthanthrene derivatives and two anthanthrene derivatives (Figure 1). Ground- and excited-state absorption spectra, fluorescence spectra, excited-state lifetimes, and triplet-triplet annihilation are presented among other properties.

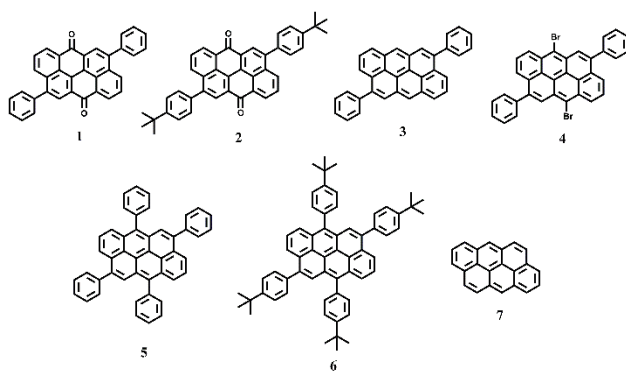


**Figure 1.** Structures of the molecules studied.

## Experimental

**Instrumentation.** Ground-state UV/vis absorption spectra were measured on a Cary 5000 spectrophotometer. Luminescence spectra were obtained using an Edinburgh Instruments FLS980 spectrometer equipped with a 450 W xenon lamp and a Hamamatsu R928P side window photomultiplier in a cooled housing ( $-20^{\circ}\text{C}$ ). Fluorescence quantum yields were obtained using the FLS980 equipped with an integrating sphere and were corrected for reabsorption of the sample.<sup>24</sup> Time-correlated single-photon counting (also on the FLS980) was utilized to determine fluorescence lifetimes. The samples were excited using a 60 ps laser diode at 404 nm. Data were analyzed using a reconvolution software package provided by Edinburgh Instruments. All experiments were performed at room temperature. A Cary Eclipse spectrometer was used to obtain phosphorescence spectra in gated delay mode.

Ultrafast transient absorption measurements were performed using a modified version of the femtosecond pump-probe UV-VIS spectrometer described elsewhere.<sup>25</sup> Briefly, 4 mJ, 45 fs pulses at 785 nm at 1 kHz repetition rate were obtained from a cryogenically-cooled, Ti:Sapphire regenerative amplifier (KM Labs Wyvern 1000-10). Approximately 5% (0.2 mJ) was reflected into the experiment, which was split into pump and probe (90 and 10%, respectively) by a beam splitter. The pump beam was directed into a frequency doubler (CSK Super Tripler) and then was focused into the sample. The probe beam was delayed in a computer-controlled optical delay (Newport MM4000 250 mm linear positioning stage) and then focused into a sapphire plate to generate white light continuum. The white light was then overlapped with the pump beam in a 2 mm quartz cuvette and then coupled into a CCD detector (Ocean Optics S2000 UV-VIS). Data acquisition was controlled by software developed by Ultrafast Systems LLC.

Nanosecond transient absorption measurements were carried out using a Q-switched Nd:YAG laser (Quantel Vibrant, pulse width ca. 5 ns) with an internal optical parametric oscillator for wavelength tunability. Pulse fluences of up to  $8\text{ mJ cm}^{-2}$  at the excitation wavelength were typically used. The transient absorption system was an Edinburgh Instruments LP920, equipped with a housed 450 W xenon lamp, Hamamatsu R928 PMT or Hamamatsu G5852-23 InGaAs photodiode, Tektronix TDS 3012C Digital Storage Oscilloscope, and an Andor iStar ICCD camera. Electronic synchronization was controlled by the provided Edinburgh Instruments F900 software. Laser excitation of the samples were aligned 90 degrees relative to the white light probe beam which passed through the sample, then through a Czerny-Turner monochromator (300 mm focal length, 1800 grooves/mm grating, 500 nm blaze,  $< 2\text{ nm}$  bandwidth) before being passed to the PMT. Spectra in the visible region were obtained with the ICCD camera, while spectra near infrared region were obtained with the InGaAs photodiode by compiling data taken in five nm increments from 900 – 1950 nm. When covering large wavelength ranges, spectra were collected in smaller increments with appropriate long-pass filters to prevent wavelength doubling. Specifically, a 494 nm long-pass filter was used from 600 – 900 nm, a 750 nm long-pass filter from 900 – 1400 nm, and a 1335 nm long-pass filter from 1400 – 2000 nm. These spectra were then stitched together to generate the full spectrum.

**Materials and Methods.** High purity solvents were obtained from commercial vendors and used as received. Tris(2,2'-bipyridyl)dichlororuthenium(II) hexahydrate was purchased from Sigma-Aldrich and converted to the hexafluorophosphate salt  $[\text{Ru}(\text{bpy})_3(\text{PF}_6)_2]$  via ion-exchange metathesis. Anthanthrene (dibenzo[def,mno]chrysene)

was purchased from Alfa Chemistry and used as received. Compounds **1** – **6** were synthesized as described previously.<sup>26</sup>

An indirect method was used to estimate the intersystem crossing yield ( $\Phi_T$ ) by using the singlet oxygen phosphorescence yield ( $\Phi_\Delta$ ). Studies have shown a correlation between  $\Phi_\Delta$  and  $\Phi_T$ , although it should be noted the  $\Phi_\Delta$  is the lower limit for  $\Phi_T$ .<sup>27, 28</sup> Because some singlet oxygen phosphorescence originates from quenching of the singlet state of the compounds, the intersystem crossing yields are calculated using the formula,  $\Phi_T = \Phi_\Delta - (\Phi_{F,d} - \Phi_{F,a})$ , where  $\Phi_{F,d}$  and  $\Phi_{F,a}$  are the deaerated and aerated fluorescence quantum yields, respectively. Due to the difficulty of measuring deaerated samples in the integrating sphere,  $\Phi_{F,d}$  was calculated by multiplying  $\Phi_{F,a}$  by the ratio of the deaerated and aerated fluorescence lifetimes. Tetracene ( $\Phi_\Delta = 0.71$ ) and phenazine ( $\Phi_\Delta = 0.83$ ) in aerated toluene were used as standards.<sup>29</sup> To determine excited-state extinction coefficients,  $[\text{Ru}(\text{bpy})_3](\text{PF}_6)_2$  was used as a relative actinometer. Based on the literature value<sup>30</sup> for the triplet extinction coefficient at 364 nm,  $\epsilon_T$ , of  $25,400 \text{ M}^{-1} \text{ cm}^{-1}$ , and the ground state extinction coefficient of  $4,600 \text{ M}^{-1} \text{ cm}^{-1}$ , the value for the difference in extinction coefficient between the triplet and ground states,  $\Delta\epsilon_T$ , was calculated to be  $20,800 \text{ M}^{-1} \text{ cm}^{-1}$  at 364 nm in water. Decomposition of  $\text{Ru}(\text{bpy})_3\text{Cl}_2$  was observed during laser-flash photolysis in water, so the experiments were run with  $[\text{Ru}(\text{bpy})_3](\text{PF}_6)_2$  in  $\text{CH}_3\text{CN}$ . It was assumed that  $\Delta\epsilon_T$  at the maximum in  $\text{CH}_3\text{CN}$  (370 nm) was equal to the calculated value at 364 nm in water. The data were collected at low laser energies to stay in the linear regime. As the lifetime of  $\text{Ru}(\text{bpy})_3(\text{PF}_6)_2$  is relatively short, the maximum  $\Delta A$  used for the actinometry was determined from a fit of the decay trace. The  $\Delta A$  spectra of each compound collected 50 ns after excitation were used for the conversion to extinction coefficient units.

## Results and Discussion

The absorption spectra of the compounds in toluene are shown in Figure 2 and maxima and extinction coefficients are tabulated in Table 1. The anthanthrone derivatives, **1** and **2**, are characterized by significantly lower energy absorption transitions relative to the anthanthrene derivatives, with maxima at 501 and 507 nm, respectively. The observed absorption maxima are red-shifted relative to the parent anthanthrone, which has an absorption maximum at 476 nm in benzene.<sup>31</sup> The addition of two phenyl groups in **1** results in a red shift of 25 nm relative to anthanthrone. The inclusion of tert-butyl groups in the 4-position of the phenyl substituents further red shifts the absorption by 6 nm relative to **1**. The extinction coefficient of **1** at the lowest energy maximum (501 nm) is  $10,800 \text{ M}^{-1} \text{ cm}^{-1}$ . While  $n\pi^*$  transitions could be present in these anthanthrone derivatives, this transition is likely dominated by  $\pi\pi^*$  transitions due to the value of the extinction coefficient. The extinction coefficient of **2** was not obtained because of its poor solubility in toluene. The spectra of **3** – **7** are similar in shape, with sharp transitions that increase in intensity with increasing wavelength. These absorption peaks with extinction coefficients at the low energy maxima in the  $40,000 - 60,000 \text{ M}^{-1} \text{ cm}^{-1}$  range correspond to  $\pi\pi^*$  transitions. The energy of the absorption maxima in the anthanthrene derivatives decreases as the number of substituents is increased. Anthanthrene (**7**) has a  $\lambda_{\text{max}}$  of 433 nm. The inclusion of two phenyl groups in **3** decreases the absorption energy to 439 nm. The absorption  $\lambda_{\text{max}}$  is further decreased to 454 nm in **5** when the number of phenyl substituents is increased to four. The inclusion

of tert-butyl groups to the four phenyl substituents results in absorption energy of 457 nm in **6**. The bromo containing derivative, **4**, has the lowest energy absorption  $\lambda_{\text{max}}$  of 460 nm.

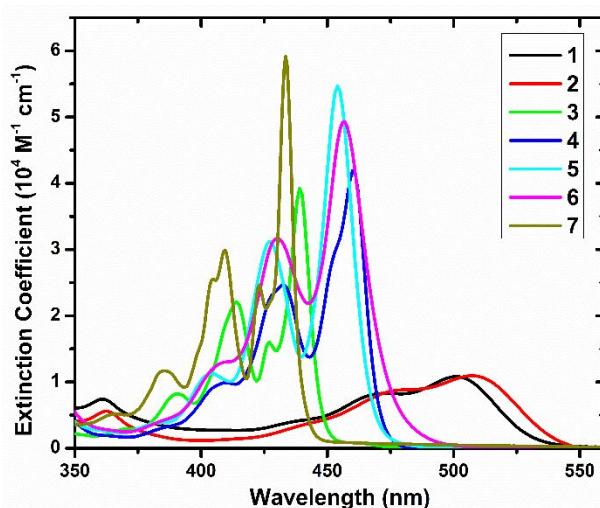


**Figure 2.** Absorption spectra of compounds in toluene. The spectrum of **2** is not in extinction coefficient units due to low solubility and is instead normalized to **1**.

Figure 3 shows the fluorescence spectra of the complexes in toluene. The fluorescence maxima ( $\lambda_{\text{em}}$ ), deaerated lifetimes ( $\tau_{\text{F}}$ ), and aerated and deaerated quantum yields ( $\Phi_{\text{F,a}}$  and  $\Phi_{\text{F,d}}$ , respectively) are listed in Table 1. Fluorescence decays and fits are shown in Figure S1. Fluorescence was not observed in compound **4** due to very fast intersystem crossing (discussed later). The fluorescence maxima of the anthanthrone derivatives red-shift along with the absorption spectra. The lifetimes and quantum yields are shorter/smaller for the anthanthrone derivatives, as fast intersystem crossing dominates the decay. Lifetimes are around 1 ns, while fluorescence quantum yields are near 10%, similar to anthanthrone.<sup>31</sup> This results in radiative rate constants on the order of  $1 \times 10^8 \text{ s}^{-1}$ . The fluorescence maxima of the anthanthrene derivatives also red-shift along with the ground state absorption spectra; the parent anthanthrene (**7**) has the highest fluorescence energy and the fluorescence of **6**, which contains four t-Bu-phenyl substituents, has the lowest fluorescence energy. The deaerated lifetimes of the anthanthrene derivatives (other than **4**) range from 2.99 – 4.40 ns, while the deaerated fluorescence quantum yields range from 0.58 – 0.84. It should be noted that these quantum yield values are significantly higher than those observed previously in methylene chloride.<sup>26</sup> It is unclear if this is due to a difference in the solvent polarity, the use of an integrating sphere with a fluorescence reabsorption correction, or some combination of the both. The radiative rate constants ( $k_{\text{r}}$ ) are all very similar, ranging from  $1.6 - 2.8 \times 10^8 \text{ s}^{-1}$ . The lifetime of **4** was measured using ultrafast transient absorption spectroscopy, and is only 40 ps (see Figure S2), again due to fast intersystem crossing.

As mentioned in the experimental section, an indirect method was used to estimate the intersystem crossing yield ( $\Phi_{\text{T}}$ ) using the singlet oxygen phosphorescence yield ( $\Phi_{\Delta}$ ).  $\Phi_{\Delta}$  represents the lower limit for  $\Phi_{\text{T}}$ <sup>27, 28</sup> and the production of singlet oxygen via the quenching of the singlet excited states must be taken into account. It should also be noted that the sum of  $\Phi_{\text{F,d}}$  and  $\Phi_{\text{T}}$  is greater than unity for some of the molecules due to the error in quantum yield measurements (15% for both  $\Phi_{\text{F,d}}$  or  $\Phi_{\text{T}}$ ). However, the observed values still provide general trends across the

series of molecules which allows for an understanding of the photophysical processes. The anthranthrones, **1** and **2**, have large  $\Phi_T$  values (Table 1) of 0.93 and 0.83, respectively. The high intersystem crossing yields give credence to the presence of  $n\pi^*$  states, in accordance with El Sayed's rule. The rate constants for intersystem crossing ( $k_{isc}$ ) are nearly an order of magnitude larger than the rates constants for radiative decay, which accounts for the low fluorescence quantum yields and short fluorescence lifetimes. Anthranthrene derivatives **3**, **5**, **6**, and **7**, all have  $\Phi_T$  values ranging from 0.24 – 0.31. As  $\Phi_T$  is smaller than  $\Phi_{F,d}$  for each, the calculated  $k_{isc}$  values are all slightly smaller than  $k_r$ . As with  $k_r$ , the values for  $k_{isc}$  for these four molecules are very comparable, highlighting the similarities in relaxation pathways from the singlet state. For these four molecules, there are not any significant trends in  $k_r$  or  $k_{isc}$  brought on by changes in structure. Compound **4** is drastically different due to the presence of bromide groups in the 6 and 12 positions, which increase  $k_{isc}$  by about two orders of magnitude via heavy-atom-induced spin-orbit coupling. Because  $k_{isc} \gg k_r$ ,  $\Phi_T$  is unity.

**Table 1.** Photophysical properties of compounds in toluene

Compound	$\lambda_{abs}/nm$	$\epsilon/10^3 M^{-1} cm^{-1}$	$\lambda_{em}/nm$	$\tau_F/ns^a$	$\Phi_{F,d}^b$	$\Phi_{F,d}^b$	$\Phi_A^b$	$\Phi_T^b$	$k_r/10^8 s^{-1}$	$k_{isc}/10^8 s^{-1}$
<b>1</b>	361, 472, 501	7.43, 8.28, 10.8	543	0.76	0.085	0.082	0.93	0.93	1.1	12
<b>2</b>	362, 479, 507	N/A <sup>c</sup>	554	1.03	0.13	0.13	0.83	0.83	1.2	7.8
<b>3</b>	414, 427, 439	22.1, 16.0, 39.2	443	4.38	0.73	0.82	0.40	0.31	1.9	0.71
<b>4</b>	410, 432, 460	9.91, 24.6, 41.9	N/A <sup>d</sup>	0.04 <sup>e</sup>	N/A <sup>d</sup>	N/A	1	1	N/A <sup>d</sup>	250
<b>5</b>	404, 427, 454	11.3, 31.2, 54.7	463	3.17	0.71	0.82	0.35	0.24	2.6	0.76
<b>6</b>	410, 430, 457	13.0, 31.7, 49.3	467	2.97	0.77	0.84	0.35	0.28	2.8	0.94
<b>7</b>	385, 409, 433	11.7, 29.9, 59.1	435	3.57	0.48	0.58	0.41	0.31	1.6	0.87

<sup>a</sup>10% error, <sup>b</sup>15% error, <sup>c</sup>Not soluble enough to obtain reliable extinction coefficient, <sup>d</sup>Fluorescence is too weak to obtain values, <sup>e</sup>Obtained from fs transient absorption.

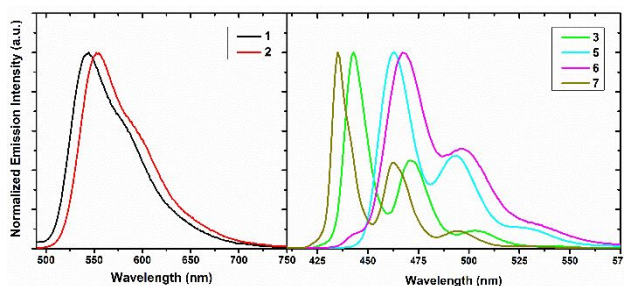


**Figure 3.** Normalized emission spectra of **1** and **2** (left) and **3**, **5**, **6**, and **7** (right) in toluene.  $\lambda_{ex}$  (nm): **1** (450), **2** (450), **3** (380), **5** (400), **6** (400), **7** (380).

The ultrafast transient absorption spectra are given in supporting information (SI) Figures S3 – S9 with relevant properties in Table S1. All samples were excited at 400 nm and the transient spectra were measured to six nanoseconds. For **1** and **2**, absorption maxima at time zero are observed at wavelengths longer than 650 nm, with bleaches observed at shorter wavelengths due to a combination of stimulated emission and ground-state absorption. The maxima blue shift over the first several picoseconds, via what is likely intramolecular vibrational relaxation. The shift is larger for **2**, and the reason for this is unclear, although the slightly red-shifted emission relative to **1** could decrease the intensity of the blue edge of the peak leading to an arbitrarily large shift. Following the slight blue shifts, shorter wavelength maxima grow in with spectra similar to the long time scale spectra (discussed later). These lifetimes are consistent with those observed for the fluorescence decay. Compounds **3** – **7** show similar trends with long wavelength maxima that, in general, blue shift followed by further shifts corresponding to formation of the

triplet state. As mentioned above, **4** rapidly forms the triplet state via large  $k_{isc}$  with only one lifetime observed (Figure S2). The other anthanthrene derivatives all show two lifetimes with the first being longer (20 – 128 ps) than that observed for **1** and **2**. It is still assumed this first lifetime corresponds to vibrational relaxation, and is followed by the longer lifetime corresponding to fluorescence and intersystem crossing (and nonradiative decay when competitive with  $k_r$  and  $k_{isc}$ .)

The extinction coefficient difference between the triplet-excited state and ground state ( $\Delta\epsilon_T$ ) can be determined using a relative actinometer. In this case,  $[\text{Ru}(\text{bpy})_3](\text{PF}_6)_2$  in deaerated  $\text{CH}_3\text{CN}$  solution was used with a calculated  $\Delta\epsilon_{\text{Ru}}$  of  $20,800 \text{ M}^{-1} \text{ cm}^{-1}$  at 370 nm (see experimental), and it was assumed that  $\Phi_T$  for  $[\text{Ru}(\text{bpy})_3](\text{PF}_6)_2$  is unity. When samples are absorbance matched at the excitation wavelength, equation 1 can be used to determine  $\Delta\epsilon_T$ , where  $\Delta A_X$  is the maximum absorption difference of the unknown compound at a given wavelength,  $\Delta A_{\text{Ru}}$  is the maximum absorption difference of the  $\text{Ru}(\text{bpy})_3(\text{PF}_6)_2$ ,  $\Phi_T$  is the intersystem crossing yield for the unknown compound, and  $\eta_X$  and  $\eta_{\text{Ru}}$  are the refractive indices of the solvents of the unknown sample and the  $\text{Ru}(\text{bpy})_3(\text{PF}_6)_2$  sample, respectively.

$$\Delta\epsilon_T = \frac{\Delta\epsilon_{\text{Ru}}(\Delta A_X/\Delta A_{\text{Ru}}) \eta_X^2}{\Phi_T \eta_{\text{Ru}}^2} \quad (1)$$

The transient absorption difference spectra in extinction coefficient units are shown in Figures 4 (**1** and **2**) and 5 (**3 – 7**) with relevant properties listed in Table 2. The spectra of the anthanthrones, **1** and **2**, were obtained in deuterated benzene to allow for transparency in the NIR region that toluene does not provide (Note: the actinometry experiments were performed in toluene and these  $\Delta\epsilon_T$  values were used to generate the benzene- $d_6$  spectra in Figure 4). The spectra are quite remarkable, with positive absorption features observed to nearly two  $\mu\text{m}$ . The shapes of the spectra of both **1** and **2** are quite similar due to their similar structures, with only minor shifts in the peak maxima observed. Relative to **1**, the peak maxima of **2** undergo slight bathochromic shifts in the visible and slight hypsochromic shifts in the NIR. The intensity of the absorption peaks is impressive, with  $\Delta\epsilon_T$  values over  $27,000 \text{ M}^{-1} \text{ cm}^{-1}$  in the visible and reaching  $2,100$  and  $3,500 \text{ M}^{-1} \text{ cm}^{-1}$  in the NIR for **1** and **2**, respectively. The triplet-triplet absorption spectra of the anthanthrones, **3 – 7**, were collected in toluene and also have similar band shapes but show significant shifts in absorption peak maxima as the structures change. The trends in excited-state absorption energies are identical to those observed in the ground state for the phenyl substituted anthanthrones; the  $\lambda_{\text{max}}$  for anthanthrene (**7**) occurs at the highest energy and the  $\lambda_{\text{max}}$  for the anthanthrene containing four, t-butyl phenyl substituents (**6**) occurs at the lowest energy. The excited state  $\lambda_{\text{max}}$  for the bromo substituted complex falls in the middle of the series. The  $\Delta\epsilon_T$  values are relatively similar, ranging from  $17,000 – 29,000 \text{ M}^{-1} \text{ cm}^{-1}$  at the long-wavelength maxima.

The triplet excited-state energies (Table 2) were obtained using 77 K phosphorescence measurements in 2:2:1:1 diethyl ether:iodoethane:ethanol:toluene (Figure S10). The anthanthrones, **1** and **2**, possess nearly identical triplet energies with values of 1.58 and 1.57 eV, respectively. These values are  $> 0.1 \text{ eV}$  larger than any of the triplet energies obtained for the anthanthrones. This observation coupled with the dramatically lower singlet state energies of the anthanthrones result in singlet-triplet energy gaps for the anthanthrones that are nearly half of those calculated for the anthanthrones! The triplet state energies of the anthanthrene derivatives are all within 0.06 eV. Interestingly,

the change in the triplet-triplet absorption peak maxima relative to **7** are significantly larger (0.12 (**3**) – 0.19 (**6**)). This implies the energies of the upper triplet excited states are more affected by the changes in molecular structure than the  $T_1$  states. Further, there is a substituent dependent trend in the magnitude of the singlet-triplet energy gap in the anthanthrenes. Anthanthrene (**7**) possesses the largest singlet-triplet gap in the series. The singlet-triplet gap of the anthanthrene with four, *t*-butyl substituted phenyl groups (**6**) has the smallest singlet-triplet gap in the series. The results indicate that excited-state extinction coefficients, absorption maxima, and triplet energies can be readily tuned by inclusion of substituents.

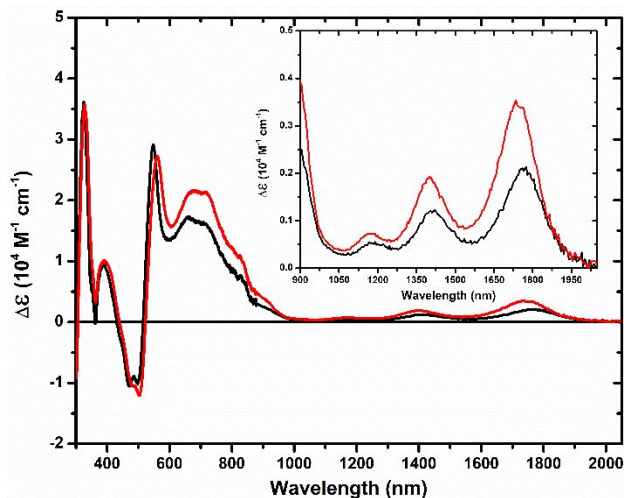


**Figure 4.** Transient absorption difference spectra of **1** (black) and **2** (red) in benzene- $d_6$ .  $\lambda_{\text{ex}} = 355$  nm

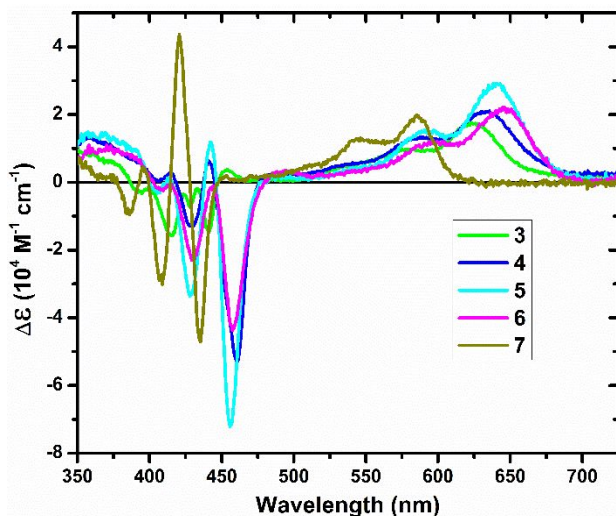


**Figure 5.** Transient absorption difference spectra of **3** – **7** in toluene.  $\lambda_{\text{ex}} = 450$  nm (**3** – **6**), 438 nm (**7**).

Because long-lived triplet states are present, triplet-triplet annihilation (TTAn) is a possible decay pathway. This is supported by observing delayed fluorescence as a function of laser pulse energy (Figure S11). The spectra are distorted relative to those in Figure 3 because the samples are concentrated and significant reabsorption of the emitted photons occurs. When monitoring at a constant time delay and varying the laser pulse energy, the delayed fluorescence intensity decreases as the laser energy decreases. To prove the delayed fluorescence originates from TTA, the dependence of the integrated intensity on the incident laser pulse energy was also evaluated (Figure 6 for **1**, Figure S12 for **2**, **3**, **5** – **7**). The integrated delayed fluorescence intensity was proportional to the square of the laser pulse energy. Double logarithm plots inset in Figures 6 and S12 yield straight lines with slopes ranging from 1.70 – 2.10, indicating the delayed fluorescence signal originates from TTAn.<sup>32-34</sup> It should be noted that for **4**, the extent of TTAn relative to the other molecules is significantly less due to its short triplet lifetime (see below). Although delayed fluorescence is shown for **4** in Figure S11, much higher laser energies had to be used to observe signal. These higher energies induce nonlinear absorption behavior, which results in unreliable plots of delayed fluorescence intensity versus laser pulse energy.<sup>35</sup> Due to the behavior of the other six derivatives, it is still assumed the delayed fluorescence signal for **4** is produced via TTAn.

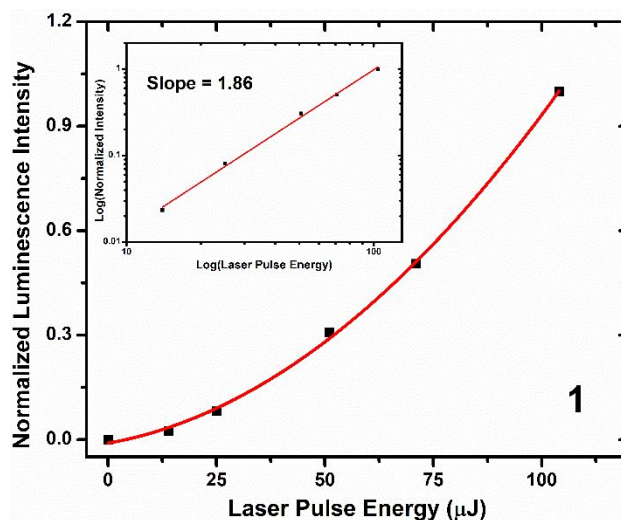


**Figure 6.** Normalized delayed integrated fluorescence intensity of **1** as a function of incident pulse energy in deaerated toluene. The data were integrated over the range shown in Figure S11 (475 – 700 nm) and normalized to the highest integrated intensity. The solid line is the best quadratic fit. Inset: double logarithm plot of the same data, with slope listed.

By knowing  $\Delta\epsilon_T$  for all molecules, the time-resolved data in  $\Delta A$  units can be converted to triplet concentration ( $[^3M^*]$ ) vs time ( $t$ ) traces, which can then be used to calculate both the triplet-state lifetime ( $\tau_T = 1/k_T$ ) and the triplet-triplet annihilation rate constant ( $k_{TT}$ ) using equation 2, where  $[^3M^*]_0$  is the triplet concentration at time zero.<sup>36</sup> Fits of the data are shown in Figures 7 (**1**) and S13 (**2-7**) and results listed in Table 2. It is useful to examine the trends in  $\tau_T$  in relation to  $\Phi_T$ . In general, the molecules with the largest  $\Phi_T$  also have the smallest  $\tau_T$ . Because both processes involve intersystem crossing, this is expected. Therefore, **4** has the shortest triplet lifetime, followed by **1** and **2**, then the other anthanthrene derivatives. While **3**, **5**, **6**, and **7** do not explicitly follow this trend,  $\tau_T$  is shorter for **3** and **7** (larger  $\Phi_T$ ) and longer for **5** and **6** (smaller  $\Phi_T$ ). For these,  $\tau_T$  also increases as the molecules become larger. Particularly interesting are the values for  $k_{TT}$ . For the anthanthrones, **1** and **2**, these values are very similar, with nearly diffusion control limited values. The value of  $k_{TT}$  for **7** is similar to **1** and **2** and consistent with previous results,<sup>37</sup> but as the anthanthrenes become larger, the values begin to decrease. Indeed, there is nearly an order of magnitude difference in  $k_{TT}$  between the unsubstituted anthanthrene (**7**) and the most sterically encumbered (**6**) with the others falling between them. The results suggest steric bulk inhibits annihilation, as observed previously.<sup>17-19, 38</sup> It is curious that **1** and **2** have similar values to **7** despite the difference in steric bulk, but the difference in the nature of the excited states (anthanthrone vs anthanthrene) may play a role.

$$[^3M^*] = \frac{[^3M^*]_0 e^{-k_T t}}{1 + [^3M^*]_0 (k_{TT}/k_T) (1 - e^{-k_T t})} \quad (2)$$

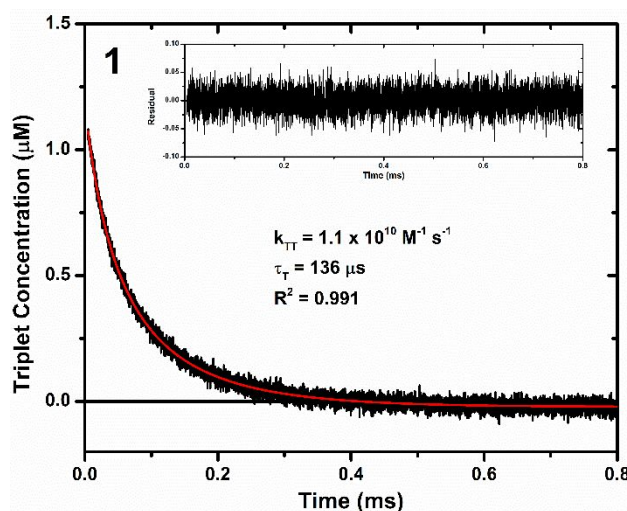


**Figure 7.** Triplet concentration of **1** as a function of time following 464 nm excitation fit to eq 2. Signal was detected at 545 nm. Inset: residual as a function of time.

**Table 2.** Transient absorption properties of **1** – **7** in toluene unless otherwise noted.

Compound	$\lambda_T/\text{nm}$	$\epsilon/10^4 \text{ M}^{-1} \text{ cm}^{-1}$	$E_T/\text{eV}^b$	$\Delta E_{S-T}/\text{eV}$	$\tau_T/\mu\text{s}$	$k_{TT}/10^9 \text{ M}^{-1} \text{ s}^{-1}$
<b>1</b>	547/662/1760 <sup>a</sup>	2.9/1.7/0.21	1.58	0.74	140	11
<b>2</b>	561/676/1735 <sup>a</sup>	2.7/2.2/0.35	1.57	0.72	180	9.6
<b>3</b>	577/624	0.98/1.7	1.45	1.31	580	3.9
<b>4</b>	587/632	1.3/2.1	1.39	1.24	31	4.4
<b>5</b>	591/640	1.6/2.9	1.41	1.23	880	4.2
<b>6</b>	598/646	1.2/2.2	1.41	1.17	1200	1.6
<b>7</b>	543/585	1.3/2.0	1.46	1.34	380	12

<sup>a</sup>In benzene-d<sub>6</sub>, <sup>b</sup>Obtained from 77 K phosphorescence in 2:2:1:1 diethyl ether:iodoethane:ethanol:toluene, <sup>c</sup>Singlet energies estimated using the wavelength at 10% of the peak intensity on the low-energy side of the ground-state absorption maxima

## Conclusions

These anthanthrene and anthanthrone derivatives have absorption and emission features that can be readily tuned by the addition of substituents, which typically red shift both the absorption and emission features. In general, increasing the number of substituents increases the extent of the red shifts. For all molecules the lifetimes of the singlet state are controlled by competition between  $k_r$  and  $k_{isc}$ . The anthanthrone derivatives, which likely possess  $n\pi^*$  singlet states, rapidly undergo intersystem crossing to the triplet state with quantum yields greater than 0.8, yielding relatively small fluorescence quantum yields. The anthanthrene derivatives (other than **4**) have much more comparable values of  $k_r$  and  $k_{isc}$ , with  $k_r$  being two to five times larger. This leads to  $\Phi_F$  values from 0.58 – 0.84, with  $\Phi_T$  values from 0.24 – 0.31. Because **4** possesses heavy bromine atoms, intersystem crossing is approximately two orders of magnitude faster than radiative decay due to spin-orbit coupling, resulting in unity  $\Phi_T$ . For the anthanthrone derivatives, the triplet-triplet absorption spectra are broad and intense in the visible, with weaker transitions observed to nearly two  $\mu\text{m}$ . For the anthanthrene derivatives, the triplet-triplet absorption spectra follow the trend in the ground-state absorption with red-shifts observed as the number of substituents increases. Once in the triplet state, the molecules can decay via vibrational relaxation or triplet-triplet annihilation. The lifetimes of the

triplet state,  $\tau_T$ , trend with  $\Phi_T$ ; **4** has the shortest lifetime, followed by the anthanthrone derivatives, likely caused by spin-orbit coupling and the presence of  $n\pi^*$  states, respectively. For the other anthanthrene derivatives,  $\tau_T$  gets slightly longer as substituents are added to the molecules. Finally,  $k_{TT}$  is near the diffusion controlled limit in the anthanthrone derivatives and anthanthrene (**7**), but decreases across the anthanthrene series as the steric bulk in the molecules increases because collisions resulting in annihilation are inhibited.

**Corresponding Author**

\*E-mail: david.stewart.32.ctr@us.af.mil, joy.haley.1@us.af.mil

**ACKNOWLEDGEMENT**

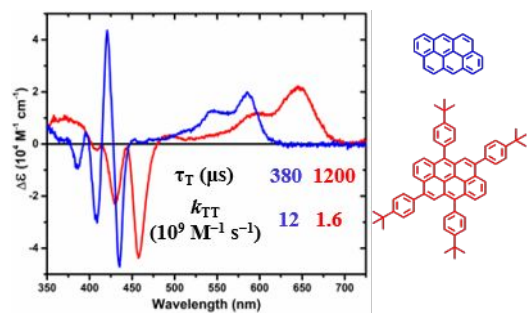
Funding support was provided by AFRL/AFOSR and AFRL/RX Directorates, Air Force Research Laboratory.

**Electronic Supplementary Information:** Fluorescence decay traces and fits, ultrafast transient absorption difference spectra and lifetimes, 77 K phosphorescence spectra, delayed fluorescence spectra as a function of laser energy, integrated delayed fluorescence as a function of laser energy with double logarithm plots, triplet concentration as a function of time with fits to eq 2.

## REFERENCES

1. L. W. Tutt and T. F. Boggess, *Prog. Quantum Electron.*, 1993, **17**, 299-338.
2. Z.-B. Liu, Y.-F. Xu, X.-Y. Zhang, X.-L. Zhang, Y.-S. Chen and J.-G. Tian, *J. Phys. Chem. B*, 2009, **113**, 9681-9686.
3. J. W. Perry, K. Mansour, S. R. Marder, K. J. Perry, D. Alvarez, Jr. and I. Choong, *Optics Letters*, 1994, **19**, 625-627.
4. J. W. Perry, *Nonlinear Optics of Organic Molecules and Polymers*, 1997, 813-840.
5. W. Blau, H. Byrne, W. M. Dennis and J. M. Kelly, *Opt. Commun.*, 1985, **56**, 25-29.
6. W. Su, T. M. Cooper and M. C. Brant, *Chem. Mater.*, 1998, **10**, 1212-1213.
7. R. L. Sutherland, M. C. Brant, J. Heinrichs, J. E. Rogers, J. E. Slagle, D. G. McLean and P. A. Fleitz, *J. Opt. Soc. Am. B*, 2005, **22**, 1939-1948.
8. P. K. Hegde, A. V. Adhikari, M. G. Manjunatha, C. S. S. Sandeep and R. Philip, *Synth. Met.*, 2009, **159**, 1099-1105.
9. B. Gu, K. Lou, H.-T. Wang and W. Ji, *Opt. Lett.*, 2010, **35**, 417-419.
10. S. Venugopal Rao, T. Shuvan Prashant, D. Swain, T. Sarma, P. K. Panda and S. P. Tewari, *Chem. Phys. Lett.*, 2011, **514**, 98-103.
11. J. E. Ehrlich, S. P. Ananthavel, S. Barlow, K. Mansour, K. Mohanalingam, S. R. Marder, J. W. Perry, M. Rumi and S. Thayumanavan, *MCLC S&T, Sect. B: Nonlinear Opt.*, 2001, **27**, 121-131.
12. I. Carmichael and G. L. Hug, *J. Phys. Chem. Ref. Data*, 1986, **15**, 1-250.
13. R. Bonneau, I. Carmichael and G. L. Hug, *Pure Appl. Chem.*, 1991, **63**, 289-299.
14. K. A. Nguyen, J. Kennel and R. Pachter, *J. Chem. Phys.*, 2002, **117**, 7128-7136.
15. A. P. Darmanyan, *Chem. Phys. Lett.*, 1984, **110**, 89-94.
16. T. J. Kemp and J. P. Roberts, *Trans. Faraday Soc.*, 1969, **65**, 725-731.
17. R. Kunieda, M. Fujitsuka, O. Ito, M. Ito, Y. Murata and K. Komatsu, *J. Phys. Chem. B*, 2002, **106**, 7193-7199.
18. Z. Liu, Z. Bian, F. Hao, D. Nie, F. Ding, Z. Chen and C. Huang, *Org. Electron.*, 2009, **10**, 247-255.
19. V. K. Rai, M. Nishiura, M. Takimoto, S. Zhao, Y. Liu and Z. Hou, *Inorg. Chem.*, 2012, **51**, 822-835.
20. V. K. Rai, M. Nishiura, M. Takimoto and Z. Hou, *J. Mater. Chem. C*, 2013, **1**, 677-689.
21. J. Sun, J. Yang, C. Zhang, H. Wang, J. Li, S. Su, H. Xu, T. Zhang, Y. Wu, W.-Y. Wong and B. Xu, *New J. Chem.*, 2015, **39**, 5180-5188.
22. N. A. Kukhta, T. Matulaitis, D. Volyniuk, K. Ivaniuk, P. Turyk, P. Stakhira, J. V. Grazulevicius and A. P. Monkman, *J. Phys. Chem. Lett.*, 2017, **8**, 6199-6205.
23. K. A. Hodgkinson and I. H. Munro, *J. Mol. Spectrosc.*, 1973, **48**, 57-71.
24. K. Suzuki, A. Kobayashi, S. Kaneko, K. Takehira, T. Yoshihara, H. Ishida, Y. Shiina, S. Oishi and S. Tobita, *Phys. Chem. Chem. Phys.*, 2009, **11**, 9850-9860.
25. A. V. Nikolaitchik, O. Korth and M. A. J. Rodgers, *J. Phys. Chem. A*, 1999, **103**, 7587-7596.
26. B. K. Shah, D. C. Neckers, J. Shi, E. W. Forsythe and D. Morton, *J. Phys. Chem. A*, 2005, **109**, 7677-7681.
27. S. Cekli, R. W. Winkel, E. Alarousu, O. F. Mohammed and K. S. Schanze, *Chem. Sci.*, 2016, **7**, 3621-3631.
28. A. Parthasarathy, S. Goswami, T. S. Corbitt, E. Ji, D. Dascier, D. G. Whitten and K. S. Schanze, *ACS Appl. Mater. Interfaces*, 2013, **5**, 4516-4520.
29. F. Wilkinson, W. P. Helman and A. B. Ross, *J. Phys. Chem. Ref. Data*, 1993, **22**, 113-262.
30. C. Creutz, M. Chou, T. L. Netzel, M. Okumura and N. Sutin, *J. Am. Chem. Soc.*, 1980, **102**, 1309-1319.
31. L. Viaene, H. Van Mingroot, P. Van Haver, M. Van der Auweraer, F. C. De Schryver, A. Itaya and H. Masuhara, *J. Photochem. Photobiol., A*, 1992, **66**, 1-13.
32. J. B. Birks, *Photophysics of Aromatic Molecules*, 1970, **74**, 1294-1295.

33. D. V. Kozlov and F. N. Castellano, *Chem. Commun.*, 2004, **0**, 2860-2861.
34. W. Zhao and F. N. Castellano, *J. Phys. Chem. A*, 2006, **110**, 11440-11445.
35. R. L. Sutherland, *Handbook of Nonlinear Optics*, Taylor & Francis, 2003.
36. T. N. Singh-Rachford and F. N. Castellano, *Coord. Chem. Rev.*, 2010, **254**, 2560-2573.
37. S. K. Sugunan, C. Greenwald, M. F. Paige and R. P. Steer, *J. Phys. Chem. A*, 2013, **117**, 5419-5427.
38. A. C. Benniston, A. Harriman, S. L. Howell, C. A. Sams and Y.-G. Zhi, *Chem. - Eur. J.*, 2007, **13**, 4665-4674.



Excited-state absorption, triplet lifetimes, and triplet-triplet annihilation rate constants can be tuned by structural modifications.